

SCIENTIFIC REPORTS



OPEN

High-Performance Wrap-Gated InGaAs Nanowire Field-Effect Transistors with Sputtered Dielectrics

Received: 31 July 2015
Accepted: 09 October 2015
Published: 26 November 2015

Li-Fan Shen^{1,3}, SenPo Yip^{2,3,4}, Zai-xing Yang^{2,3,4}, Ming Fang^{2,4}, TakFu Hung², Edwin Y.B. Pun^{1,3} & Johnny C. Ho^{2,3,4}

Although wrap-gated nanowire field-effect-transistors (NWFETs) have been explored as an ideal electronic device geometry for low-power and high-frequency applications, further performance enhancement and practical implementation are still suffering from electron scattering on nanowire surface/interface traps between the nanowire channel and gate dielectric as well as the complicated device fabrication scheme. Here, we report the development of high-performance wrap-gated InGaAs NWFETs using conventional sputtered Al₂O₃ layers as gate dielectrics, instead of the typically employed atomic layer deposited counterparts. Importantly, the surface chemical passivation of NW channels performed right before the dielectric deposition is found to significantly alleviate plasma induced defect traps on the NW channel. Utilizing this passivation, the wrap-gated device exhibits superior electrical performances: a high I_{ON}/I_{OFF} ratio of $\sim 2 \times 10^6$, an extremely low sub-threshold slope of 80 mV/decade and a peak field-effect electron mobility of $\sim 1600 \text{ cm}^2/(\text{Vs})$ at $V_{DS} = 0.1 \text{ V}$ at room temperature, in which these values are even better than the ones of state-of-the-art NWFETs reported so far. By combining sputtering and pre-deposition chemical passivation to achieve high-quality gate dielectrics for wrap-gated NWFETs, the superior gate coupling and electrical performances have been achieved, confirming the effectiveness of our hybrid approach for future advanced electronic devices.

In the past decade, III–V compound semiconductor nanowires (NWs) have attracted extensive amount of research and development interest due to their excellent physical properties for high-performance nanoelectronics and highly efficient photovoltaics^{1–10}. Among many III–V NW materials, InAs has been demonstrated with the superior field-effect electron mobility (μ) as well as the gigahertz device operation^{11–13}. However, further applications are still restricted by the substantial leakage current in InAs-based devices because of its small electronic band gap^{14,15}. Recently, ternary InGaAs NWs with uniformly tunable chemical stoichiometries have been successfully illustrated as the alternative device channel material, and the relatively larger band gap reduces the leakage issue but not the electron mobility^{16–21}. At the same time, a newly developed gate-all-around (GAA) device architecture with a coaxial wrap gate completely surrounding the NW channel is also frequently adopted. The capacitive coupling between the gate and the NW is increased in order to reduce the OFF current (I_{OFF}) and improve the sub-threshold slope (SS)

¹Department of Electronic Engineering, City University of Hong Kong, 83 Tat Chee Avenue, Kowloon, Hong Kong.

²Department of Physics and Materials Science, City University of Hong Kong, 83 Tat Chee Avenue, Kowloon, Hong Kong. ³State Key Laboratory of Millimeter Waves, City University of Hong Kong, 83 Tat Chee Avenue, Kowloon, Hong Kong.

⁴Shenzhen Research Institute, City University of Hong Kong, Shenzhen, China. Correspondence and requests for materials should be addressed to J.C.H. (email: johnnyho@cityu.edu.hk) or E.Y.B.P. (email: eeybpun@cityu.edu.hk)

through the enhanced electrostatic gate control over the channel^{22–25}. It is noted that this wrap-gated (WG) device geometry depends on the conformal deposition of high-quality and ultrathin (i.e. ~ 10 nm) high- κ dielectric layer all over the NW, in which the resulting device characteristics are strongly affected by the obtained dielectric/NW interface qualities; as a result, atomic layer deposition (ALD) is typically employed for this critical dielectric coating step despite its high processing cost, long reaction time, and limited material choices for the dielectrics²⁶.

Both vertical and lateral WG NW device configurations have been reported for InAs^{27–33}. Wernersson *et al.* provided a comprehensive investigation of vertical WG InAs NW field-effect transistors (FETs) with the HfO₂ gate dielectric, delivering a maximum ON current density of 0.08 A/mm with an SS of 75 mV/dec at room temperature³⁴. This SS value is very close to the theoretical limit of SS = 60 mV/dec, indicating good control of channel electrostatics and interface properties. However, electron beam lithography was required to pattern growth seeds at specified locations for the vertical NW synthesis on underlying crystalline III–V substrates²⁷, together with complicated device fabrication process with numerous lithography and etching steps²⁸, all these made the implementation of these vertical device structures challenging. On the other hand, Deshmukh and his coworkers attained lateral InAs WG NWFETs with only two lithography steps and without any etching requirement, the devices exhibit a respectable ON-OFF current ratio (I_{ON}/I_{OFF}) of 5×10^3 at $V_{DS} = 0.5$ V at room temperature and an impressive SS of 5–54 mV/dec at low temperatures (1.5 to 250 K)³⁰. During the device fabrication, it is crucial to use a low-temperature process (i.e. < 120 °C) for the HfO₂ deposition to avoid polymerizing the resist layers employed in the lithography steps. Similarly, Xu *et al.* further optimized the device performance, yielding a significantly large current density of 400 μ A/ μ m, an impressive I_{ON}/I_{OFF} of $\sim 10^4$ and a μ of 1600 cm²/(Vs) which is the highest among all WG InAs NWFETs reported so far for $V_{DS} = 0.5$ V at room temperature³³. Up to now, there have been few reports focusing on using the improved channel materials of InGaAs NWs with further simplified WG device fabrication process.

Recently, we have successfully synthesized crystalline InGaAs NWs, with a smooth surface and a low defect concentration, using a unique two-step catalytic chemical vapor deposition (CVD)¹⁸. In this work, we use the crystalline NWs to construct lateral WG NWFETs with a simple fabrication process. Notably, the high- κ gate dielectric (~ 12 nm thick Al₂O₃) can be conformally deposited around the suspended NW channel by standard sputtering, which is a simple, attractive and economic process to deposit dielectrics in industry. Combining with the pre-deposition surface passivation of NWs by self-assembly sulfur-containing monolayer such as ammonium sulfide ((NH₄)₂S), the fabricated devices are found to display improved dielectric/NW interface properties, exhibiting excellent electrical performances such as a small I_{OFF} below 1 pA, a high I_{ON}/I_{OFF} ratio of $\sim 2 \times 10^6$, a low SS of 80 mV/dec, and an excellent μ approaching 1600 cm²/(Vs) at $V_{DS} = 0.1$ V at room temperature. This superior capacitive gate coupling of WG InGaAs NWFETs confirms the versatility of our simplified WG device fabrication scheme using high-quality sputtered dielectrics, as well as the potential applications of InGaAs NW channels for future high-speed, low-power, and high-frequency electronic devices.

Results

The InGaAs NWs, synthesized by the two-step catalytic CVD method in this work, are dense, long (> 10 μ m), and straight with the smooth surface, as shown in the scanning electron microscope (SEM) image in Fig. 1a. In order to evaluate the crystallinity of the as-grown NWs, high-resolution transmission electron microscopy (HRTEM) are performed on a representative NW, as illustrated in Fig. 1b. Based on the plane spacing determination and the reciprocal lattice spots extracted by fast Fourier transform (FFT), the NW exhibits single-crystalline zinc-blende (ZB) structure with a dominant growth orientation in the $\langle 111 \rangle$ direction, and no significant amount of stacking faults or twin-plane polytypic defects are found in the samples. The spacing between the adjacent lattice planes are found to be 0.34 and 0.21 nm, which are in good agreement with the plane spacing of (111) and (022) equivalent planes in the In-rich thin-film counterparts, respectively³⁵. Also, the NW stoichiometry can be assessed using the corresponding energy-dispersive X-ray spectroscopic (EDS) spectrum depicted in Fig. 1c. The In concentration x , being 0.58 in our ternary In _{x} Ga _{$1-x$} As NWs, is consistent with our previous work in controlling the NW composition by varying the precursor source powder ratio¹⁷.

Next, the WG InGaAs NWFETs can be fabricated by a simple process as presented in Fig. 2. Briefly, the as-prepared NWs are first drop-casted onto the SiO₂/p⁺-Si substrate (50 nm thick thermally grown oxide) pre-coated with a layer of 100 nm thick lift-off resist (LOR). After the NW deposition, another stack of LOR / photoresist (100 nm / 500 nm thick) layer is spin-coated to form a sandwiched structure (Fig. 2a). Standard photolithography is then employed to define the source/drain (S/D) electrodes, followed by Ni evaporation (150 nm thick) and lift-off process, with the purpose to achieve a suspended NW structure (Fig. 2b). Here, this suspended structure is soaked in (NH₄)₂S (stock solution) for 40 s, carefully rinsed in DI water and anhydrous ethanol, and baked at 120 °C for 5 hours in order to passivate the exposed NW surface. A second photolithography step is then performed to outline the WG region, and a ~ 12 nm thick Al₂O₃ high- κ dielectric layer is deposited around the NW by conventional sputtering with a slow deposition rate of ~ 0.5 nm/min (Fig. 2d). Finally, gate stack electrode (5 nm Ti / 90 nm Al) is sputtered with a slow deposition rate of ~ 2 nm/min at the beginning to ensure conformal contact with the Al₂O₃ layer and realize the final WG geometry (Fig. 2e,f). The substrate rotation is crucial

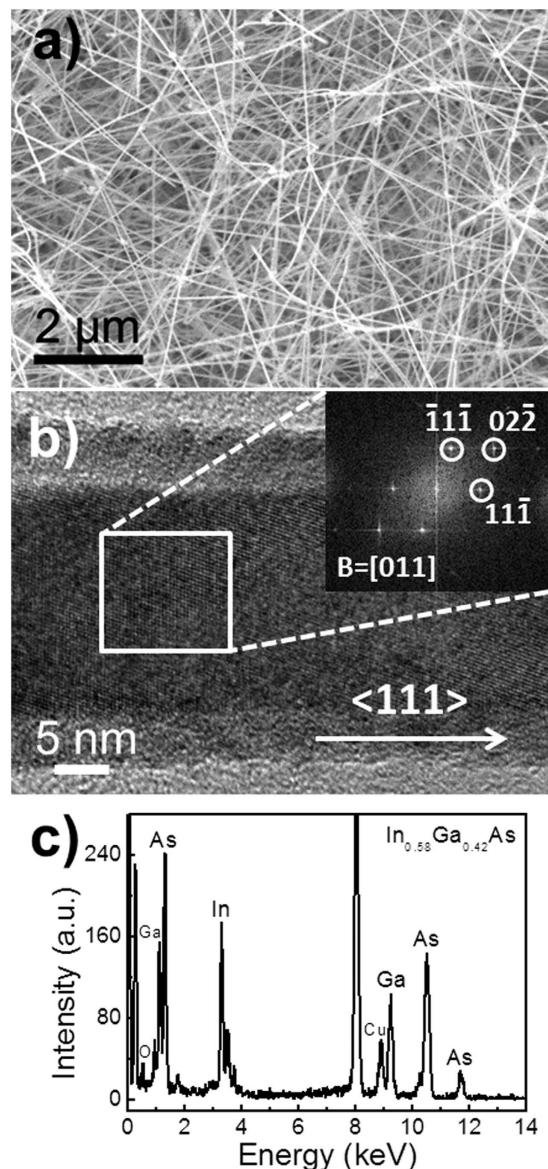


Figure 1. (a) Electron microscopy characterization of the as-grown InGaAs NWs; (b) High-resolution transmission electron microscope (HRTEM) image and the corresponding fast Fourier transform (FFT) of a representative NW; (c) EDS spectrum of the corresponding NW body.

throughout the deposition process in order to ensure conformal coverage of Al_2O_3 and gate stack onto the NW channel.

Figure 3a shows the illustrative schematic of the WG InGaAs NWFET constructed in this work, and Fig. 3b,c give the cross-sectional and top-view SEM images of a representative device before and after the WG fabrication, respectively. It is noted that the NW device has a typical diameter of $d \sim 29$ nm and a WG length of $L \approx 3.67$ μm (distance between source/drain ~ 6 μm). Although high-quality gate dielectrics can be often obtained by the ALD method, the ALD processing is complicated involving a lot of organometallic precursors and requiring a lot of calibrations before achieving the optimal condition. Importantly, the precursor residues may also be incorporated in the deposited films. Instead, magnetron sputtering is employed in this work to deposit the dielectric layer around the suspended NW channel, and the process is simpler, more economical, and industrial friendly than the ALD process. Moreover, sputtering is also more compatible with temperature sensitive flexible substrates³⁶, enabling the fabrication of mechanically flexible high-performance WG devices. With the aim to inspect the electrical property of the sputtered Al_2O_3 dielectric obtained here, simple metal-oxide-semiconductor (MOS) capacitors are fabricated on highly doped p-Si (100) substrate with a resistivity of 0.001 to 0.005 ohm-cm utilizing the same sputtered Al_2O_3 dielectric and Al metal electrode. Based on the high-frequency (1 MHz) capacitance–voltage (C–V) measurement (Supplementary Information Figure S1a), the dielectric constant of sputtered Al_2O_3 is determined to be 7.216, which is similar to the value attained by typical ALD process, confirming the

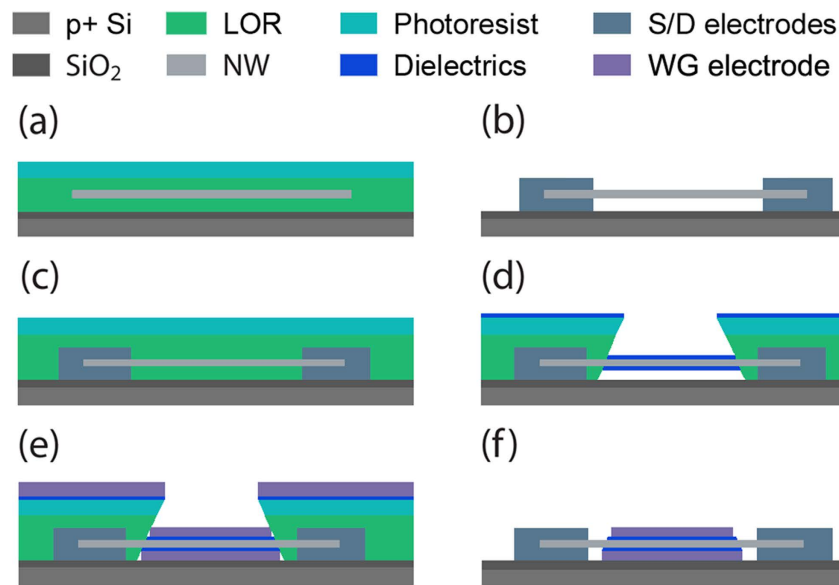


Figure 2. Schematic diagrams for the fabrication process of InGaAs wrap-gated NWFET devices. (a) Sandwiched NW between lift-off resists covered by a layer of photoresist; (b) S/D electrodes defined by lithography and processed with the $(\text{NH}_4)_2\text{S}$ passivation; (c) Spin-coated with LOR and photoresist; (d) Window opened by lithography and Al_2O_3 thin film deposited homogeneously by sputtering; (e) Deposition of Ti/Al gate metal by sputtering; (f) Final lift-off.

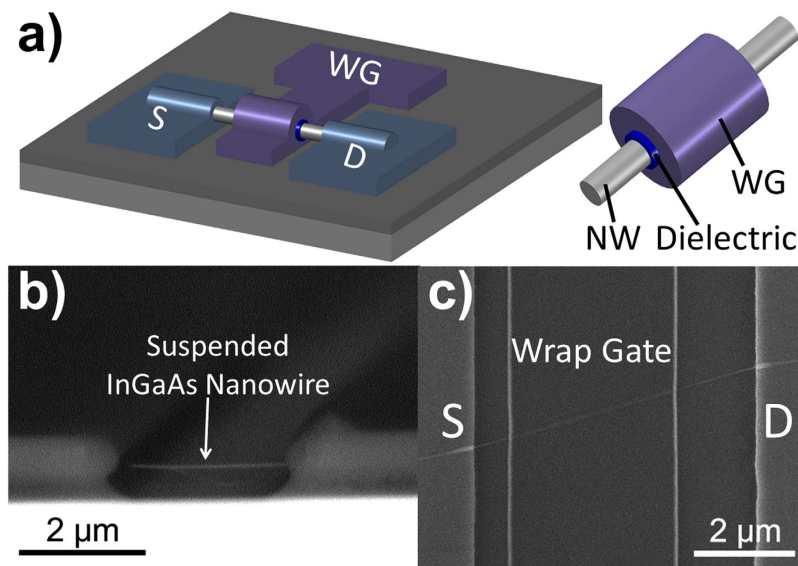


Figure 3. (a) Illustrative schematic of the InGaAs wrap-gated NWFET device; (b) SEM image of a suspended InGaAs NW channel; (c) SEM image of a representative InGaAs wrap-gated NWFET fabricated.

excellent dielectric quality of the sputtered Al_2O_3 layer used in this work. Furthermore, this dielectric layer also increases the ON current density and minimizes the hysteresis effect of the fabricated device by isolating the NW channel from the external environment, and improves the overall device performance and reliability (Supplementary Information Figure S1b)³.

The plasma generated during the sputter deposition of Al_2O_3 can damage the NW channel surface by inducing significant amount of surface/interface defect trap states³⁷. In order to reduce this negative impact, the surface passivation of III-V NWs by sulfur based chemicals such as ammonium sulfide $(\text{NH}_4)_2\text{S}$ have been commonly adopted in other applications, in order to enhance the device performance by improving the SS and increasing the μ ^{38–42}. Thus, in this work, we employ similar chemical passivation technique with the intention to alleviate the detrimental effect of the plasma induced surface defects here. In details, as shown in Figure 4a, the influence of $(\text{NH}_4)_2\text{S}$ passivation on the InGaAs NW

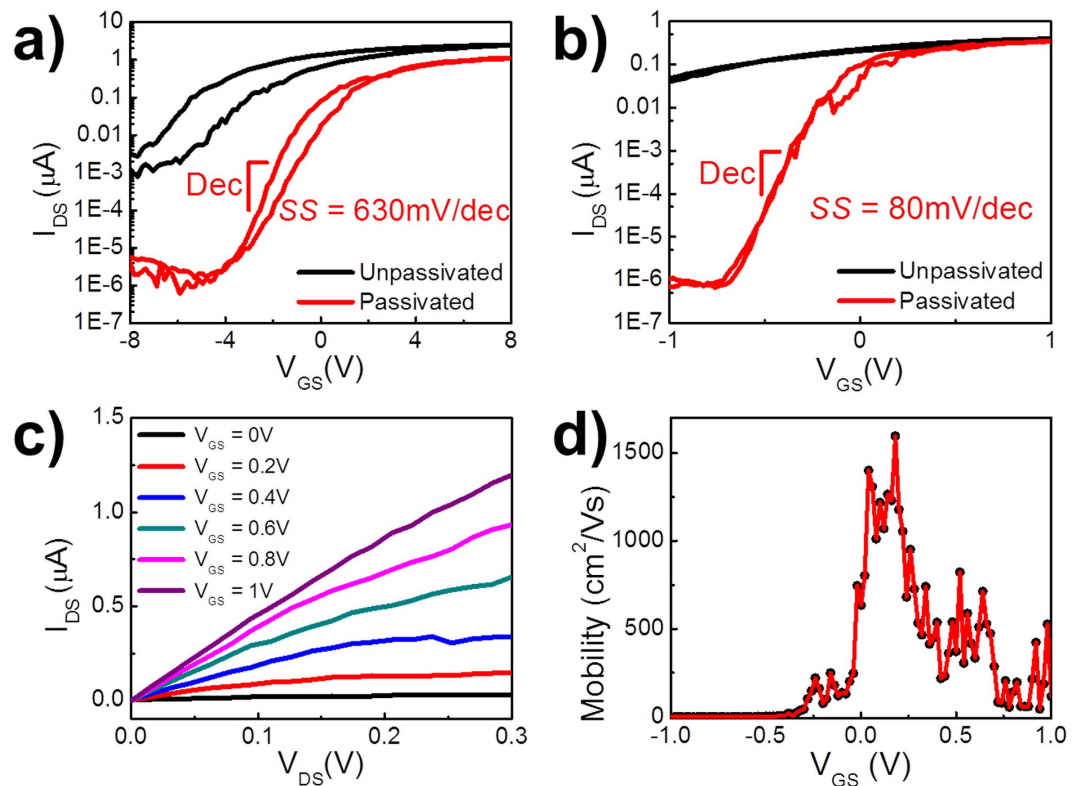


Figure 4. (a) Transfer characteristics of the back-gated InGaAs NWFET before and after passivation in logarithmic scale at $V_{DS} = 0.1\text{V}$; (b) Transfer characteristics of the InGaAs wrap-gated NWFET with and without passivation in logarithmic scale at $V_{DS} = 0.1\text{V}$. (c) Output characteristics of the InGaAs wrap-gated NWFET device processed with passivation; (d) Mobility assessment of InGaAs wrap-gated NWFET device processed with passivation under $V_{DS} = 0.1\text{V}$ at room temperature.

electrical properties is investigated, and the electrical performance of back-gated NWFET before (unpassivated) and after passivation (passivated) is evaluated. It can be clearly seen that after passivation the I_{OFF} is reduced significantly and the ON current (I_{ON}) does not change much. Hence, surface passivation does enhance the device I_{ON}/I_{OFF} by at least two orders of magnitude and decrease the SS by half, which can be attributed to the saturation of surface states on the NW channel surface⁴³. Accordingly, the device hysteresis can also be reduced by isolating the NW surface from the ambient environment⁴⁴.

As presented in Fig. 4b, when the passivation scheme is applied to the WG device fabrication, the performance enhancement is even more profound due to the larger dielectric/channel interfacial area and better electrostatic gate control. After passivation, the I_{OFF} is decreased drastically and the electrical properties such as SS and I_{ON}/I_{OFF} are all improved, indicating the significance of surface passivation for the WG device geometry. The device exhibits n-type conduction with a minimal hysteresis under low-voltage operation ($V_{DS} = 0.1\text{V}$), and an extremely small OFF current ($I_{OFF} = 0.4\text{pA}$) with $V_{GS} = -1\text{V}$, and $\sim 1\text{ }\mu\text{A}$ ON current with $V_{GS} = 1\text{V}$ with a high I_{ON}/I_{OFF} ratio of $\sim 2 \times 10^6$ at room temperature are obtained. Different back-gate bias with $V_{BG} = 0, 2, 4\text{V}$ are also applied to the WG device (see Supplementary Information Figure S2), and a negligible influence of V_{BG} on the electrical performance of WG devices is observed, indicating the dominant gate control of the WG here. Figure 4c presents the linear I_{DS} - V_{DS} behavior of the same WG device under $V_{DS} = 0.1\text{V}$ after passivation, which confirms the ohmic-like contact formation with Ni S/D electrodes and suggests that the passivation process has no adverse effect on the contact properties of the devices.

As an important parameter for low-power and high-speed operations, SS characterizes how fast a FET can be switched, and is defined as $SS = dV_{GS}/d\log I_{DS}$, and the steep sub-threshold slope indicates a faster transition between the device OFF and ON states⁴⁵. Although sputtered Al_2O_3 dielectric is employed in this work, the fabricated InGaAs WG NWFET exhibits a good SS of 80mV/dec with $V_{DS} = 0.1\text{V}$ at room-temperature approaching the theoretical limit of 60mV/decade , and is even smaller than the recently reported values of ALD enabled InAs WG NWFETs^{32,33,46}, as shown in Fig. 4b. It is also noted that many of our fabricated devices display SS values below 200mV/dec with $V_{DS} = 0.1\text{V}$, illustrating the effectiveness of our combined sputter deposition and chemical passivation approach in achieving high-quality dielectric layers (Supplementary Information Figure S3).

	I_{ON}/I_{OFF}	SS (mV/dec)	Peak Transconductance (μ S)	Peak Mobility ($\text{cm}^2/(\text{Vs})$)
Back-gated devices	54000	1000	0.18	1050
Wrap-gated devices	340000	200	1.59	1300

Table 1. Compilation and comparison of average on-off ratio, sub-threshold slope (SS), peak transconductance and peak field-effect electron mobility between back-gated (without any surface passivation) and wrap-gated devices.

The corresponding field-effect electron mobility of the InGaAs WG NWFET can also be assessed by the standard square law model as demonstrated in Fig. 4d:

$$\mu = \frac{L^2}{C_{OX}} \frac{dG_g}{dV_{GS}}, \quad (1)$$

where L is the length of the gate, G_g is the conductance of the nanowire channel covered by the gate and C_{OX} is the gate capacitance obtained from a finite element analysis software COMSOL tailored for this wrap-gated geometry with the details given in the Supplementary Information Figure S4 and S5. The C_{OX} determined from the simulation gives a relatively accurate gate capacitance, together with the known gate length and diameter, the field-effect mobility of the NW can be calculated reliably¹². It should be noted that there is always a thin native oxide layer of ~ 2.5 nm on the NW surface¹⁸, which would be subtracted from the measured NW diameters to give the effective channel width for subsequent mobility determination. As the G_g is only attributed to the conductance of gate coverage area and the two ungated segments in the channel are not controlled by the gate, the conductance of these two ungated parts (G_1 and G_2) which are independent of V_{GS} can be deduced from the total conductance of the nanowire (G_t). We assume that when the current nearly saturates, flat band condition occurs and the NW conducts homogeneously in the entire channel. The conductance of the two ungated parts can then be calculated by using the following equation:

$$G_{1(2)} = \frac{L_t G_t}{L_{1(2)}}, \quad (2)$$

where $L_{1(2)}$ is the length of the ungated segment, and L_t is the total length of the nanowire in the channel. The total conductance (G_t) can be expressed by

$$\frac{1}{G_t} = \frac{1}{G_1} + \frac{1}{G_g} + \frac{1}{G_2}. \quad (3)$$

With the conductance of the two ungated parts G_1 and G_2 , the conductance G_g can be calculated by the following equation:

$$G_g = \frac{G_t G_1 G_2}{G_1 G_2 - G_1 G_t - G_2 G_t}. \quad (4)$$

The peak transconductance $\left(g_m = \frac{dG_g}{dV_g} \Big|_{V_{DS}} \right)$ for the representative WG NWFET device (Figure 4b,d) is found to be $2.52 \mu\text{S}$ and the calculated peak μ is $\sim 1600 \text{ cm}^2/(\text{Vs})$ at room temperature, which is comparable to the lately reported state-of-the-art InAs WG NWFET³³.

To evaluate the performance enhancement between the back-gated (without any surface passivation) and WG NWFETs, several device parameters such as I_{ON}/I_{OFF} , sub-threshold slope, peak transconductance, and peak field-effect electron mobility of the devices are compiled and compared in Table 1 (see details in Supplementary Information Table S1 and Table S2). The average I_{ON}/I_{OFF} of WG devices is found to be $\sim 3.4 \times 10^5$, which is an order of magnitude higher than the value of back-gated devices ($\sim 5.4 \times 10^4$). The SS of WG devices varies from 80 to 300 mV/dec and the average values is estimated to be ~ 200 mV/dec, which is much smaller than that of ~ 1000 mV/dec for back-gated devices. Moreover, the average peak transconductance of the WG devices is also significantly higher than that of other back-gated devices, and all these improved device performances indicate the excellent capacitive gate coupling of the WG NWFETs fabricated in this work.

Discussion

Although WG NWFETs have been explored as an ideal FET geometry for low-power and high-frequency applications, the required performance improvement and practical device implementation still lag behind expectation, largely due to the electron scattering at the NW surface and/or interface traps between

the NW channel and gate dielectric, and the complicated device fabrication scheme. The current work adopts a hybrid approach, combining the well-established sputter deposition to achieve high-quality Al_2O_3 dielectric layers and the pre-deposition surface passivation of NW channels by self-assembly sulfur-containing monolayer in the device fabrication of InGaAs WG NWFETs. The devices are all fabricated using single-crystalline ternary InGaAs NWs with tunable chemical stoichiometry, smooth surface and low defect concentration using a simple process with standard photolithography and electrode deposition. The high- κ gate dielectric Al_2O_3 layer is deposited homogeneously around the NW channel by conventional sputtering, which is a more economic industrial friendly process as compared to the typical ALD scheme in obtaining the dielectrics. The pre-sputtering chemical passivation by $(\text{NH}_4)_2\text{S}$ is also employed to alleviate the detrimental effect of the plasma induced surface/interface defect trap states on the NW channels. After passivation, the InGaAs WG NWFETs exhibits excellent electrical properties, with a high $I_{\text{ON}}/I_{\text{OFF}}$ ratio of $\sim 2 \times 10^6$, a low SS of 80 mV/decade, a small I_{OFF} of 0.4 pA, and a peak field-effect mobility of $\sim 1600 \text{ cm}^2/(\text{Vs})$ at $V_{\text{DS}} = 0.1 \text{ V}$ at room temperature, which is comparable to or even better than state-of-the-art ALD enabled WG NWFETs^{30,32,33}. Further improvement could be achieved by employing the aromatic thiolate (ArS^-) based molecular monolayers as the surface modification of NWs in this wrap-gated device fabrication, since this ArS^- surface processing can not only decrease the amount of surface traps for the better mobility but also induce the surface electronic charge to move the device V_{th} positively³⁸. The superior capacitive gate coupling of WG NWFETs and the improved electrical performance, including the low leakage current and steep sub-threshold slope, suggest the technological potential of our sputtering enabled WG NWFETs for future high-speed, low-power, and high-frequency electronic devices.

Method

Nanowire Synthesis. InGaAs nanowires (NWs) used in this study were synthesized in a two-zone horizontal tube furnace by using a solid-source chemical vapor transport method as previously reported¹⁸. Briefly, the SiO_2/Si growth substrate (50 nm thermal oxide on degenerately boron doped Si (100) with a resistivity of 0.001 to 0.005 ohm-cm) was pre-deposited with a 0.5 nm thick Au film as the catalyst in thermal evaporator, and then positioned in the downstream zone of the furnace. InAs (99.999% purity) and GaAs (99.999% purity) powders were mixed in 1:1 weight ratio and loaded into a boron nitride crucible in the upstream zone. Hydrogen (99.9995%) was used as carrier gas to transport the evaporated source materials to the growth substrate. A two-step growth method was adopted to ensure the uniform NW morphology and stoichiometry¹⁷. During the growth, the flow rate of H_2 was maintained at 100 sccm and the corresponding pressure downstream is ~ 1 Torr. After the growth, the source and substrate heater were stopped together and the grown NWs were taken out of the furnace after the system was cooled naturally to room temperature under the hydrogen flow.

Material Characterizations. All material characterizations were performed on the NWs obtained in the 0–1 cm region of growth substrates in order to establish a consistent study. Surface morphologies of the grown NWs were examined with a scanning electron microscope (SEM, FEI/Philips XL30 ESEM-FEG). HRTEM image was observed with a JEOL 2100F transmission electron microscope. The composition of NWs was determined using an energy dispersive X-ray spectroscopy (EDS) detector attached to the JEOL 2100F to measure the chemical composition of the grown NWs. In the EDS measurements, around thirty NWs were randomly chosen as candidates for the EDS point scan in the NW body.

Nanowire FET Fabrication and Measurements. After CVD growth, the InGaAs NWs were first harvested by sonication in high-purity ethanol solution, and then the InGaAs NW field-effect-transistors (FETs) were fabricated based on both back-gated and wrap-gated FET configuration. For the fabrication of back-gated NWFETs, the obtained NW suspension was randomly drop-casted onto pre-cleaned highly boron doped Si (100) with a resistivity of 0.001 to 0.005 ohm-cm with a 50 nm thick thermally grown gate oxide, and then spin-coated with LOR and AZ5206 photoresist and exposed to ultraviolet light and went through developing. After we delineated the source and drain patterns, a 50 nm thick Ni film was thermally deposited as the contact electrodes followed by a lift-off process.

For wrap-gated NWFETs, the InGaAs NWs were drop-casted onto the SiO_2/Si substrates which were pre-spin coated by a layer of 100 nm thick LOR, and then spin-coated with LOR and AZ5206 photoresist respectively to form a sandwiched NW between lift off resists, as schematically shown in Fig. 2(a). Photolithography was then utilized to define the source and drain regions, and a 150-nm thick Ni film was thermally deposited as the contact electrodes followed by a lift-off process. Figure 2(b) illustrates the NW is suspended between the electrodes in the developed region, and this suspended configuration was confirmed by the SEM image of a suspended InGaAs NW in Fig. 3(b). Then the devices were soaked in $(\text{NH}_4)_2\text{S}$ solution (stock solution) for 40 s in order to passivate the surface of NWs. After passivation, the devices were rinsed carefully using DI water and ethanol and baked at 120 °C for ~ 5 h. A second photolithography was performed to define the wrap-gate regions, and a dielectric layer of ~ 12 nm thick Al_2O_3 was deposited homogeneously around the NW by DC sputtering with Al metal target in oxygen and argon ambient (O_2 to Ar ratio 1.5:25) and then the devices were baked at 100 °C for ~ 5 h, as presented

in Fig. 2(c,d). After that, 5 nm Ti and 90 nm Al were deposited isotropically in a DC sputtering system as the gate electrodes followed by a lift-off process (Fig. 2(e,f)). Electrical performance of the fabricated NWFET devices was characterized with a standard electrical probe station and an Agilent 4155C semiconductor analyzer at room temperature. High-frequency (HF) capacitance-voltage (C-V) measurements were performed using HP4284A precision LCR meter.

References

- Duan, X. *et al.* High-performance thin-film transistors using semiconductor nanowires and nanoribbons. *Nature* **425**, 274–278 (2003).
- Duan, X., Huang, Y., Cui, Y., Wang, J. & Lieber, C. M. Indium phosphide nanowires as building blocks for nanoscale electronic and optoelectronic devices. *Nature* **409**, 66–69 (2001).
- Han, N. *et al.* Tunable electronic transport properties of metal-cluster-decorated III–V nanowire transistors. *Adv. Mater.* **25**, 4445–4451 (2013).
- Law, M., Greene, L. E., Johnson, J. C., Saykally, R. & Yang, P. Nanowire dye-sensitized solar cells. *Nat. Mater.* **4**, 455–459 (2005).
- Mohseni, P. K. *et al.* Monolithic III–V nanowire solar cells on graphene via direct van der waals epitaxy. *Adv. Mater.* **26**, 3755–3760 (2014).
- Thathachary, A. V., Agrawal, N., Liu, L. & Datta, S. Electron Transport in Multigate $\text{In}_x\text{Ga}_{1-x}\text{As}$ Nanowire FETs: From Diffusive to Ballistic Regimes at Room Temperature. *Nano Lett.* **14**, 626–633 (2014).
- Wallentin, J. *et al.* InP nanowire array solar cells achieving 13.8% efficiency by exceeding the ray optics limit. *Science* **339**, 1057–1060 (2013).
- Yang, Z.-x. *et al.* Surfactant-assisted chemical vapour deposition of high-performance small-diameter GaSb nanowires. *Nat. Commun.* **5** (2014).
- Shin, H. W. *et al.* Short-wavelength infrared photodetector on Si employing strain-induced growth of very tall InAs nanowire arrays. *Sci. Rep.* **5** (2015).
- Tomioka, K., Yoshimura, M. & Fukui, T. A III–V nanowire channel on silicon for high-performance vertical transistors. *Nature* **488**, 189–192 (2012).
- Guo, N. *et al.* Anomalous and highly efficient InAs nanowire phototransistors based on majority carrier transport at room temperature. *Adv. Mater.* **26**, 8203–8209 (2014).
- Ford, A. C. *et al.* Diameter-dependent electron mobility of InAs nanowires. *Nano Lett.* **9**, 360–365 (2009).
- d’Hollosy, S. *et al.* Giga-Hertz quantized charge pumping in bottom gate defined InAs nanowire quantum dots. *Nano Lett.* **15**, 4585–4590 (2015).
- Dayeh, S. A., Yu, E. T. & Wang, D. Transport coefficients of InAs nanowires as a function of diameter. *Small* **5**, 77–81 (2009).
- Fu, M. *et al.* Electrical characteristics of field-effect transistors based on indium arsenide nanowire thinner than 10 nm. *Appl. Phys. Lett.* **105**, 143101 (2014).
- Hou, J. J. *et al.* Diameter dependence of electron mobility in InGaAs nanowires. *Appl. Phys. Lett.* **102**, 093112 (2013).
- Hou, J. J. *et al.* Stoichiometric effect on electrical, optical, and structural properties of composition-tunable $\text{In}_x\text{Ga}_{1-x}\text{As}$ nanowires. *ACS Nano* **6**, 9320–9325 (2012).
- Hou, J. J. *et al.* Synthesis and characterizations of ternary InGaAs nanowires by a two-step growth method for high-performance electronic devices. *ACS Nano* **6**, 3624–3630 (2012).
- Hertenberger, S. *et al.* High compositional homogeneity in In-rich InGaAs nanowire arrays on nanoimprinted SiO_2/Si (111). *Appl. Phys. Lett.* **101** (2012).
- Jung, C. S. *et al.* Composition and phase tuned InGaAs alloy nanowires. *J. Phys. Chem. C* **115**, 7843–7850 (2011).
- Guo, Y.-N. *et al.* Polarity-driven nonuniform composition in InGaAs nanowires. *Nano Lett.* **13**, 5085–5089 (2013).
- Shirak, O., Shtempluck, O., Kotchtakov, V., Bahir, G. & Yaish, Y. High performance horizontal gate-all-around silicon nanowire field-effect transistors. *Nanotechnology* **23**, 395202 (2012).
- Del Alamo, J. A. Nanometre-scale electronics with III–V compound semiconductors. *Nature* **479**, 317–323 (2011).
- Si, M. *et al.* Effects of forming gas anneal on ultrathin InGaAs nanowire metal-oxide-semiconductor field-effect transistors. *Appl. Phys. Lett.* **102**, 093505 (2013).
- Franklin, A. D. *et al.* Carbon nanotube complementary wrap-gate transistors. *Nano Lett.* **13**, 2490–2495 (2013).
- Leskelä, M. & Ritala, M. Atomic layer deposition chemistry: recent developments and future challenges. *Angew. Chem. Int. Edit.* **42**, 5548–5554 (2003).
- Egard, M. *et al.* Vertical InAs nanowire wrap gate transistors with $f_t > 7$ GHz and $f_{\text{max}} > 20$ GHz. *Nano Lett.* **10**, 809–812 (2010).
- Thelander, C., Fröberg, L. E., Rehnstedt, C., Samuelson, L. & Wernersson, L.-E. Vertical enhancement-mode InAs nanowire field-effect transistor with 50-nm wrap gate. *IEEE Electron Device Lett.* **29**, 206–208 (2008).
- Tanaka, T. *et al.* Vertical surrounding gate transistors using single InAs nanowires grown on Si Substrates. *Appl. Phys. Expr.* **3**, 025003 (2010).
- Dhara, S. *et al.* Facile fabrication of lateral nanowire wrap-gate devices with improved performance. *Appl. Phys. Lett.* **99**, 173101 (2011).
- Storm, K., Nylund, G., Samuelson, L. & Micolich, A. P. Realizing lateral wrap-gated nanowire FETs: controlling gate length with chemistry rather than lithography. *Nano Lett.* **12**, 1–6 (2012).
- Sasaki, S. *et al.* Encapsulated gate-all-around InAs nanowire field-effect transistors. *Appl. Phys. Lett.* **103**, 213502 (2013).
- Li, Q. *et al.* Suspended InAs nanowire gate-all-around field-effect transistors. *Appl. Phys. Lett.* **105**, 113106 (2014).
- Thelander, C. *et al.* Development of a vertical wrap-gated InAs FET. *IEEE Trans. Electron Devices* **55**, 3030–3036 (2008).
- Kim, T. Strain effects and crystal structures of the $\text{In}_x\text{Ga}_{1-x}\text{As}$ active layer in the highly lattice-mismatched $\text{In}_x\text{Ga}_{1-x}\text{As}/\text{InP}$ modulation-doped coupled double quantum wells. *Solid State Commun.* **110**, 69–73 (1999).
- Carcia, P., McLean, R., Reilly, M. & Nunes Jr, G. Transparent ZnO thin-film transistor fabricated by rf magnetron sputtering. *Appl. Phys. Lett.* **82**, 1117–1119 (2003).
- Wang, F. *et al.* Surface roughness induced electron mobility degradation in InAs nanowires. *Nanotechnology* **24**, 375202 (2013).
- Cheung, H. *et al.* Modulating electrical properties of InAs nanowires via molecular monolayers. *ACS Nano* **9**, 7545–7552 (2015).
- Petrovykh, D. Y., Yang, M. J. & Whitman, L. J. Chemical and electronic properties of sulfur-passivated InAs surfaces. *Surf. Sci.* **523**, 231–240 (2003).
- Hang, Q. L. *et al.* Role of molecular surface passivation in electrical transport properties of InAs nanowires. *Nano Lett.* **8**, 49–55 (2008).
- Suyatin, D. B., Thelander, C., Bjork, M. T., Maximov, I. & Samuelson, L. Sulfur passivation for ohmic contact formation to InAs nanowires. *Nanotechnology* **18**, 105307 (2007).
- Gu, J., Neal, A. & Ye, P. Effects of $(\text{NH}_4)_2\text{S}$ passivation on the off-state performance of 3-dimensional InGaAs metal-oxide-semiconductor field-effect transistors. *Appl. Phys. Lett.* **99**, 152113 (2011).

43. Dayeh, S. A., Soci, C., Paul, K., Edward, T. Y. & Wang, D. Transport properties of InAs nanowire field effect transistors: The effects of surface states. *J. Vac. Sci. Technol. B* **25**, 1432–1436 (2007).
44. Miao, J. *et al.* Single InAs nanowire room-temperature near-infrared photodetectors. *ACS Nano* **8**, 3628–3635 (2014).
45. Ferain, I., Colinge, C. A. & Colinge, J.-P. Multigate transistors as the future of classical metal-oxide-semiconductor field-effect transistors. *Nature* **479**, 310–316 (2011).
46. Wernersson, L.-E., Thelander, C., Lind, E. & Samuelson, L. III-V nanowires—Extending a narrowing road. *Proc. IEEE* **98**, 2047–2060 (2010).

Acknowledgements

We acknowledge the Early Career Scheme of the Research Grants Council of Hong Kong SAR, China (CityU 139413), the National Natural Science Foundation of China (grant number 51202205) and the Science Technology and Innovation Committee of Shenzhen Municipality (Grant JCYJ-20140419115507588) and a grant from the Shenzhen Research Institute, City University of Hong Kong.

Author Contributions

J.C.H. conceived the project. J.C.H., E.Y.B.P. and L.F.S. prepared the manuscript. L.F.S., S.P.Y. and Z.X.Y. grew the NWs. T.F.H. carried out the TEM characterization and analysis. L.F.S. and M.F. carried out the device fabrication, electrical measurements and data analysis. All authors examined and commented on the manuscript.

Additional Information

Supplementary information accompanies this paper at <http://www.nature.com/srep>

Competing financial interests: The authors declare no competing financial interests.

How to cite this article: Shen, L.-F. *et al.* High-Performance Wrap-Gated InGaAs Nanowire Field-Effect Transistors with Sputtered Dielectrics. *Sci. Rep.* **5**, 16871; doi: 10.1038/srep16871 (2015).



This work is licensed under a Creative Commons Attribution 4.0 International License. The images or other third party material in this article are included in the article's Creative Commons license, unless indicated otherwise in the credit line; if the material is not included under the Creative Commons license, users will need to obtain permission from the license holder to reproduce the material. To view a copy of this license, visit <http://creativecommons.org/licenses/by/4.0/>